Materials Research Express

PAPER • **OPEN ACCESS**

Effect of CNT on microstructural properties of Zn_2SiO_4/CNT composite via dry powder processing

To cite this article: Kar Fei Chan *et al* 2020 *Mater. Res. Express* **7** 105601

Materials Research Express

PAPER

Effect of CNT on microstructural properties of Zn_2SiO_4/CNT composite via dry powder processing

Kar Fei Chan[1], **Mohd Hafiz Mohd Zaid**[1], **Shahira Liza**[2], **Khamirul Amin Matori**[1], **Md Shuhazlly Mamat**[1], **Mohammad Adib Hazan**[1] and **Yazid Yaakob**[1,3,*]

[1] Department of Physics, Faculty of Science, Universiti Putra Malaysia, 43400 UPM Serdang, Selangor, Malaysia
[2] TriPrem i-Kohza, Malaysia-Japan International Institute Technology, Universiti Teknologi Malaysia, 54100 Kuala Lumpur, Malaysia
[3] Microscopy Unit, Institute of Bioscience, Universiti Putra Malaysia, 43400 UPM Serdang, Selangor, Malaysia
* Author to whom any correspondence should be addressed.

E-mail: kfeichan08@gmail.com **and** yazidakob@upm.edu.my

Keywords: carbon nanotubes, zinc silicate, crystallite size, lattice strain, willemite

OPEN ACCESS

RECEIVED
18 June 2020

REVISED
27 July 2020

ACCEPTED FOR PUBLICATION
25 September 2020

PUBLISHED
7 October 2020

Abstract

This work focused on the influence of carbon nanotubes (CNT) to the microstructural properties of Zn_2SiO_4/CNT (ZSO/CNT) composite. CNT was synthesized via alcohol catalytic chemical vapor deposition (ACCVD) using cobalt oxide as catalyst and ethanol as carbon source. Zinc silicate (ZSO) glass was prepared from quenching the melted commercial waste glass bottle with zinc oxide powder. ZSO/CNT-x composites with various CNT concentration (0, 1, 2 and 3 wt%) was prepared through introducing CNT into ZSO glass via dry processing technique followed by sintering process in Argon gas (Ar) environment and atmospheric (atm) environment, respectively. FESEM, XRD and EDS were employed to determine the surface morphology, phase composition and elemental distribution of sintered sample. Crystallite trigonal willemite (Zn_2SiO_4) phase was observed from argon sintered sample and the crystallite size of willemite phase in ZSO/CNT-3/Ar showed the most reduced lattice strain of 22.85% compared to ZSO/CNT-0/Ar. In contrast, semi-crystalline phase exhibited in atmospheric sintered sample resulted in high lattice strain. It is concluded that dry powder processing and inert gas thermal treatment can be an effective technique in fabricating strain-reduced ceramics/CNT composite without alternating the domain phase. Least internal strain in crystal lattice have potential on enhancing the luminescence properties of phosphor material and lattice thermal conductivity of thermoelectric material.

1. Introduction

Application of carbon nanotubes (CNT) into ceramics matrix, forming CNT/ceramics composite with enhanced thermal [1–3], electrical [4–6], and optical [7, 8] properties drew great demand in this rapid scientific development. Dry powder processing technique was the first and commonly used in fabrication of carbon nanotubes (CNT) with different host matrix such as ceramics and metal in forming composite with enhanced properties. This process was conducted by mixing CNT and the inorganic matrix in milling or manual mixing system. Although dry powder processing faced inhomogeneous CNT dispersion and least interfacial bonding between CNT and inorganic matrix [9], researchers introduced several effective milling process [6, 10] and thermal treatment such as spark plasma sintering [11] and low pressure sintering [12], which helped to solve the bottleneck in fabricating desirable CNT composite.

Beside the enhanced properties stated above, CNT plays main role in reinforcing the mechanical properties of domain matrix with very limited amount of CNT needed [13, 14]. Mazaheri *et al* stated the improving in Vickers hardness and Young's modulus was due to the pinning effect of CNT [15]. Pinning effect of CNT was located in the grain boundary, restricting the sliding and lowered the mechanical loss. Furthermore, Bi *et al* recommended flexural strength of CNT/Al_2O_3 composite was improved with obtaining small grain size leads to strong interfacial connection between CNT and Al_2O_3 [16]. However, these studies were based on the synergetic

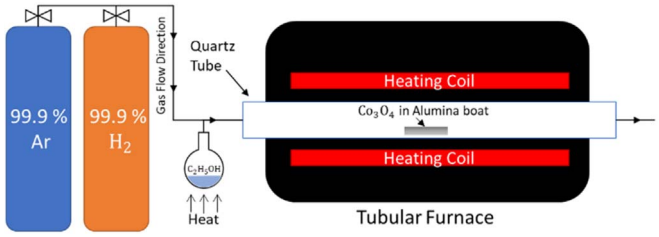

Figure 1. Schematic setup diagram for 30 min ACCVD with 50 sccm Ar and 5 sccm H_2.

effect of CNT at the grain boundary without noticing the effect of CNT towards the microstructure of the respected domain phase.

The presence of lattice strain in the microstructure of materials played significant role in mechanical performance and the phase information to the domain phase especially for glass-ceramics silica-based material. Willemite (crystallite Zn_2SiO_4) is a type of silica-based glass-ceramics which exhibited low thermal conductivity and green light emission (585 nm) with the excitation of UV. Zn_2SiO_4 exhibited glass structure at low temperature thermal treatment and initiated crystallization at high temperature [17]. When external (high temperature needed) and internal (low thermal conductivity of glassy Si-based material) factors decelerated the crystallization, crystallite size decreased in the matrix system, leaded to increase in lattice strain and low degree phase transition of glassy to crystalline phase [18, 19]. Hence, limiting lattice strain without phase modification in stable lattice dislocations of Zn_2SiO_4 potentially advancing the thermoelectric behaviour [20, 21] and narrow bandwidth emission with high quantum efficiency [22] of the material towards highly functional light emitting diode (LED) application.

In this research, we introduced the cobalt-catalysed CNT as fillers to parent zinc silicate glass powder (ZSO). Sintering process was conducted in controlled argon flow environment in reducing the lattice strain and improving the crystallite size of the crystallite phase. To show comparison with conventional glass-ceramic material synthesis process, ZSO sample with CNT addition were also sintered in atmospheric environment.

2. Materials and methodology

2.1. Materials

Ethyl alcohol (ethanol, C_2H_5OH, 99.8% AR grade, 46.07 g mol^{-1}, R&M Chemicals), Cobalt (II,III) Oxide nanopowder (Co_3O_4, <50 nm particle size, 99.5% trace metal basis, Sigma Aldrich) and Zinc oxide powder (ZnO, 99.99% metal basis, Alfa Aesar) were purchased. Waste soda lime silicate (SLS) glass bottle was harvested from commercial used ketchup bottle (Life tomato ketchup, 485 g, Region Food Industries, Malaysia).

2.2. Synthesis of carbon nanotubes (CNT)

CNT was synthesized from Co_3O_4 as metal catalyst and ethanol as carbon precursor through alcohol catalytic chemical vapor deposition (ACCVD). Co_3O_4 powder was weighed and sintered up to 800 °C with ramping rate 10 °C min^{-1} in tubular furnace with argon gas flowing (Ar, 50 sccm) in ensuring inert gas environment. At 800 °C, vaporized ethanol and hydrogen gas (H_2, 5 sccm) was introduced into the furnace for 30 min of reaction time. The sample was then annealed to ambient temperature in inert environment. ACCVD was setup as figure 1.

2.3. Parent zinc silicate glass (ZSO)

Harvested SLS glass bottle was cleaned, crushed, milled and sieved until the glass powder reached 45 μm. Micron sized SLS powder was mixed with ZnO nanopowder at ratio 1:1 and melted in electrical box furnace at 1400 °C for 3 h as figure 2. The melted SLS/ZnO liquid was water-quenched into glass fritz [17]. Glass fritz was milled into 45 μm powder labelled as ZSO glass powder.

2.4. ZSO/CNT composites via dry prowder processing

ZSO glass powder was well mixed with CNT with varying concentrations (0, 1, 2 and 3 wt%) as in table 1 and 0.5 g of mixed powder were processed with pelleting process under 5 tonnes pelleting force for 10 min using PVA as binding agent. This pelleting process produced pellet with 3.0 mm thickness. The pellet was labelled as ZSO/CNT-x as x indicated the weight percentage of CNT. The pellets was sintered in tubular furnace with Ar gas flowing at 50 sccm. The heating rate was set at 10 °C min^{-1} and held at 800 °C for 2 h. Identical pellet samples

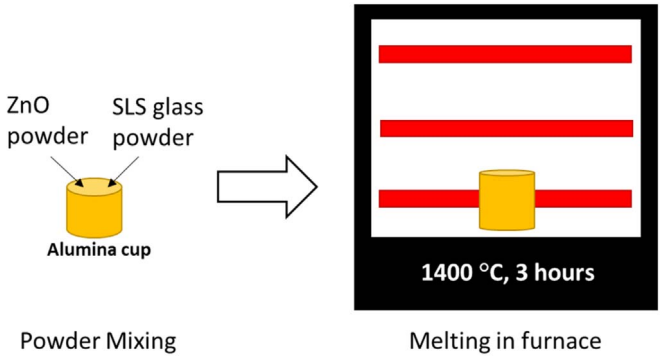

Figure 2. ZnO and SLS mixing and melting process with parameters.

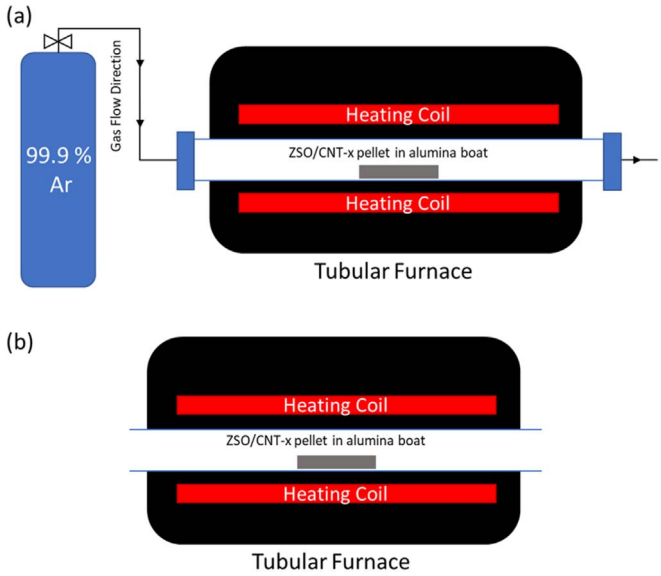

Figure 3. ZSO/CNT-x sintered for 2 h in (a) controlled Argon flow (50 sccm) and (b) atmospheric environment.

Table 1. Composition of mixed powder.

Sample	ZSO mass (g)	CNT concentration (wt%)	CNT mass (g)	CNT: ZSO
ZSO/CNT-0	20	0	0.00	0:100
ZSO/CNT-1	20	1	0.20	1:99
ZSO/CNT-2	20	2	0.40	2:98
ZSO/CNT-3	20	3	0.60	3:97

were sintered in atmospheric environment with identical sintering parameter. ZSO/CNT-x/Ar and ZSO/CNT-x/atm was labelled as sintered sample under argon gas and atmospheric environment, respectively. Figure 3 showed the setup of argon gas sintering and atmospheric sintering.

2.5. Characterization

The surface morphologies of CNT and sintered pellet samples were characterized by a field emission scanning electron microscope (FESEM, JSM-7600F, JEOL, Japan) with an Energy Dispersive x-ray Spectrometer detector (EDS, INCA, Oxford, UK) attached to observe the elemental distributions. X-ray diffractometer (XRD-6000, SHIMADZU, Japan) was utilized to determine the phase composition of samples.

2.6. Crystallite size (τ) and lattice strain (ε) calculation

Crystallite size (τ) and lattice strain (ε) of domain crystalline phase in sample were measured with Williamson-Hall equation [23] and compared with Scherrer equation [24].

By applying Williamson-Hall (W-H) equation, a correlation between crystallite size (τ_{WH}) and lattice strain (ε_{WH}) was setup. Two extra calculation had been made to W-H equation: neglecting the lattice strain ($\varepsilon_{WH} = 0$) and limiting crystallite size to infinite value ($\tau_{WH} \rightarrow \infty$). With $\varepsilon_{WH} = 0$, the W-H equation calculated crystallite size without lattice strain was labelled as τ_0. In contrast, W-H equation calculated lattice strain as crystallite size to infinite value was indicated as ε_0.

Equation (1) shows Williamson-Hall equation for crystallite size (τ_{WH}) and lattice strain (ε_{WH}) calculation. Crystallite size only (τ_0) (2) was calculated as the lattice strain was neglected and lattice strain only (ε_0) (3) was calculated as the crystallite size to infinite value.

$$\beta \cos\theta = 4\varepsilon_{WH} \sin\theta + \frac{k\lambda}{\tau_{WH}} \tag{1}$$

$$\tau_0 = \frac{k\lambda}{\beta \cos\theta}, \ \varepsilon_{WH} = 0 \tag{2}$$

$$\varepsilon_0 = \frac{\beta \cos\theta}{4 \sin\theta}, \ \tau_{WH} \rightarrow \infty \tag{3}$$

Average experimental crystallite size (τ_{exp}) (4) and strain (ε_{exp}) (5) was calculated from measured Full Width Half Maxima (β) and Bragg's angle in radian (θ) of crystallite planes, where k is the dimensionless shape factor (0.9) and λ is the wavelength of CuKα x-ray (0.154 nm).

$$\tau_{exp} = \frac{k\lambda}{\beta \cos\theta} \tag{4}$$

$$\varepsilon_{exp} = \frac{\beta}{4 \tan\theta} \tag{5}$$

3. Results and discussions

3.1. Phase composition, phase shifting and peak narrowing

XRD analysis was employed on the CNT filler, argon sintered sample (ZSO/CNT-x/Ar) and atmospheric sintered sample (ZSO/CNT-x/atm), to determine the phase compositions (refer to figures 4 and 5). Crystalline phase shifting was only observed in ZSO/CNT-x/Ar while semi-crystalline phase and amorphous phase were observed in ZSO/CNT-x/atm without phase shifting.

Phase and surface formation of CNT (CNT spectrum in figure 4) were analyzed at the first stage. Metal carbides is the well-known product from the reaction between metal and carbon. In this case shown, there is no formation of cobalt carbides from the phase spectrum. There are 3 sharp peaks found in the XRD spectrum which respect to cubic α-cobalt: 44.34°, 51.60° and 75.95° respect to (111), (002) and (020) planes. During the 30 min reaction time (800 °C), H_2 gas acted as the carrier gas for vaporized ethanol and the reducing agent onto the Co_3O_4 catalyst. The oxidation number of Co_3O_4 (can be written as $CoO{\cdot}Co_2O_3$) reduced from +2 and +3 to neutral. However, some of the reduced cobalt didn't react with the carbon atom from the vaporized ethanol remains cobalt particle without any carbon capsulation contributes to the phase of α-cobalt [25].

From figures 4, 2 h sintering process at 800 °C provided ZSO glass sufficient energy in rearranging the silicate, zinc and oxygen ion from glassy structure (water-quenched sample) into crystallite trigonal willemite phase (Zn_2SiO_4, space group = $R\bar{3}$). Impurities like magnesium (Mg) and calcium (Ca) found in SLS bottle melted and alloyed with silicate towards minor crystalline phase of tetragonal akermanite ($Ca_2MgSi_2O_7$, space group = $P\bar{4}21m$). The presence of minor ceramics in the composite: Akermanite, due to the impurities within the glass bottles during the industrial manufacturing process to improve the mechanical properties of the bottles [26]. Amorphous carbon peak and crystallite alpha-cobalt (α-Co) was found in CNT and ZSO/CNT-x/Ar. Inert gas such as Ar gas preserved the CNT from decomposing under high temperature or reacted with flowing gas. Broad peak of hexagonal carbon peak at 26° indicated crystallite graphite (002) plane which overlapped with

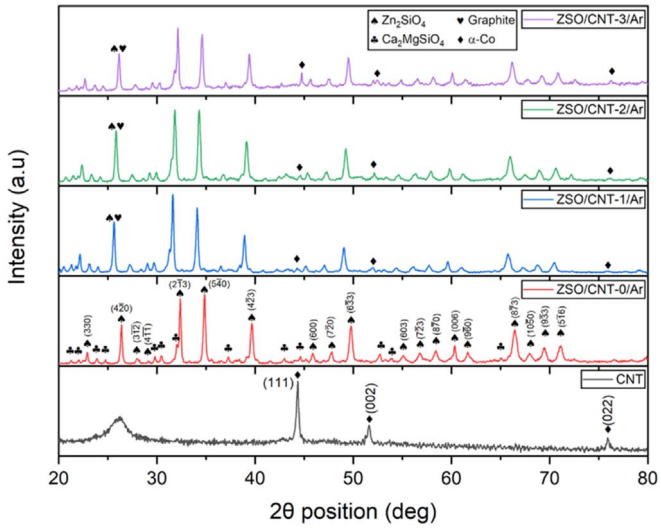

Figure 4. XRD spectrum of synthesised CNT and Argon environment sintered sample, ZSO/CNT-x Ar where x indicated the concentration of CNT.

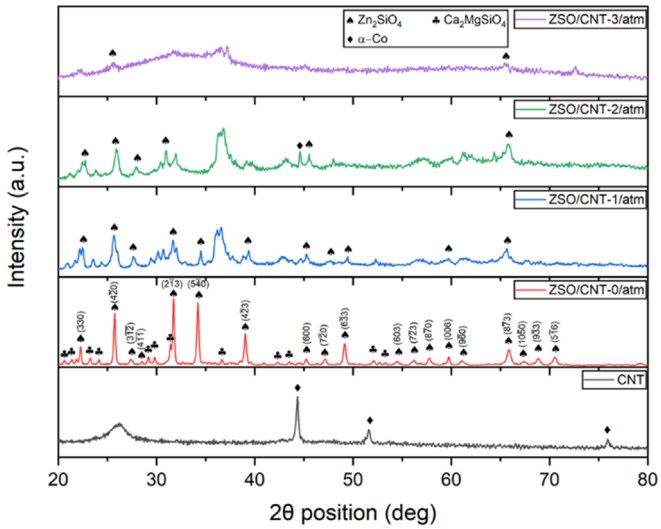

Figure 5. XRD spectrum of synthesized CNT and atmospheric environment sintered sample, ZSO/CNT-x/atm where x indicated the weight percentage of CNT.

$(4\bar{2}0)$ plane of hexagonal Zn_2SiO_4 phase. This phase overlapping phenomenon at same Bragg's angle resulted the increase of intensity at the 2θ position.

In figure 5, semi-crystalline phase existed in atmospheric sintered sample as the CNT concentration increased and amorphous phase for ZSO/CNT-3/atm sample. The possible explanation for this glassy phase formation is the decomposition of CNT under oxygen decomposition at high temperature. Near 20% oxygen contained in atmospheric air invaded the graphite layers of CNT and converted into carbon gaseous, leaving the Co particles reacted with the silicate ion in the pellet. After sintering at 800 °C for 2 h, the cobalt-silicate compound remained as glassy state, was believed the crystallite temperature of this ceramics is higher than 800 °C [27, 28].

Increasing of W-H calculated crystallite size showed relationship with phase shifting to left observed in the XRD spectrum (figure 6). Phase left-shifting indicates increased in crystallite size based on Scherrer equation. However, phase shifting is not the only parameters in crystallite size determination. In addition, the crystallite size was influenced by the β value (FWHM). FWHM values against plane of ZSO/CNT-x/Ar was plotted as in figure 7. Several major planes of crystallite willemite phase was selected in this plotting, showing the FWHM distribution of ZSO/CNT-x/Ar in the range of 0.198°–0.396° (2θ in degree). ZSO/CNT-3/Ar show the lowest FWHM distribution which is in the range of 0.198°–0.317°, resulting the largest crystallite size and lowest lattice

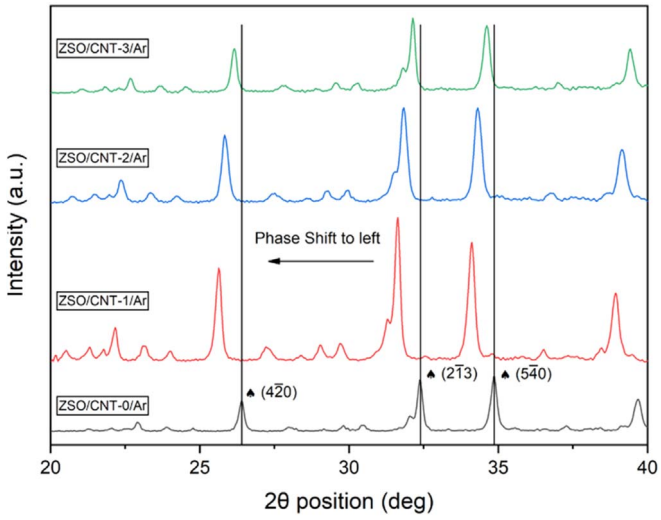

Figure 6. Phase shifting of ZSO/CNT-x/Ar respected with various CNT concentration. Phase left-shifting in XRD spectrum indicates the increasing in crystallite size based on Scherrer equation.

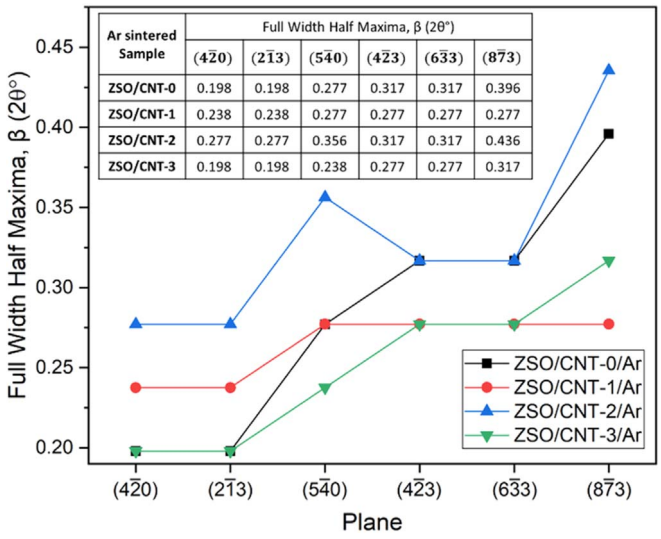

Ar sintered Sample	Full Width Half Maxima, β (2θ°)					
	(4$\bar{2}$0)	(2$\bar{1}$3)	(5$\bar{4}$0)	(4$\bar{2}$3)	(6$\bar{3}$3)	(8$\bar{7}$3)
ZSO/CNT-0	0.198	0.198	0.277	0.317	0.317	0.396
ZSO/CNT-1	0.238	0.238	0.277	0.277	0.277	0.277
ZSO/CNT-2	0.277	0.277	0.356	0.317	0.317	0.436
ZSO/CNT-3	0.198	0.198	0.238	0.277	0.277	0.317

Figure 7. FWHM distribution of major (hkl) plane in ZSO/CNT-x/Ar.

Table 2. W-H equation calculated crystallite size (τ_{WH} and τ_0 in nm) and lattice strain (ε_{WH} ($\times 10^{-3}$) and ε_0 ($\times 10^{-3}$)) of ZSO/CNT-x/Ar and Scherrer equation calculated crystallite size (τ_{exp} in nm) and lattice strain (ε_{exp} ($\times 10^{-3}$)) as comparison. Change of crystallite size and lattice strain (%) for CNT-added sample was calculated respected to ZSO/CNT-0/Ar.

	Williamson-Hall equation calculated								Scherrer equation calculated			
Ar sintered sample	τ_{WH}	ε_{WH}	τ_{WH}(%)	ε_{WH}(%)	τ_0	ε_0	τ_0(%)	ε_0(%)	τ_{exp}	ε_{exp}	τ_{exp}(%)	ε_{exp}(%)
ZSO/CNT-0	105.93	0.75	—	—	54.85	1.48	—	—	59.91	1.64	—	—
ZSO/CNT-1	111.91	0.82	+5.65	+9.93	55.29	1.53	+0.80	+3.38	58.76	1.69	−1.92	+3.00
ZSO/CNT-2	62.51	0.42	−40.99	−44.33	48.02	1.67	−12.46	+12.84	49.96	7.84	−16.61	+377.34
ZSO/CNT-3	105.13	0.58	−0.76	−22.85	61.40	1.32	+11.95	−10.81	65.12	1.49	+8.69	−9.32

strain. With applying Williamson-Hall equation (table 2), the τ_{WH} and ε_{WH} of ZSO/CNT-1/Ar showed the highest value (111.91 nm with 0.822 $\times$ 10^{-3}) while ZSO/CNT-2/Ar contributed the smallest crystallite size and strain which is 62.508 nm with 0.416 $\times$ 10^{-3} strain. With neglected the lattice strain of willemite phase, the

hexagonal phase showed the value of τ_0 similar with τ_{exp} and ZSO/CNT-3/Ar showed the crystallite size of 61.402 nm. The lattice strain of ZSO/CNT-3/Ar showed the lowest value which is 1.32×10^{-3}.

W-H calculated τ_0 and ε_0 was compared with Scherrer equation calculated τ_{exp} and ε_{exp}. The results showed similar result indicating ZSO/CNT-2/Ar has the smallest crystallite size and highest lattice strain. However, ε_{exp} and ε_0 of ZSO/CNT-2/Ar show the strain up to 377% and 12.84% compared to ZSO/CNT-0/Ar respected to the identical phase in the system. This gives the ε_0 in W-H calculation having higher accuracy in calculating the homogenous distortion in the system with the consideration of crystallite expands to infinite value while ε_{exp} calculated the average strain between phases standalone without taking the expanding of crystallite into account.

From XRD spectrum of ZSO/CNT-x/atm sample (figure 5), only crystalline willemite phase was considered in crystallite size determination. ZSO/CNT-0/atm showed τ_{WH} of 0.63×10^{-3} ε_{WH} with 109.27 nm τ_{WH}, differed 21.33% and 3.15% in lattice strain and crystallite size, as comparing to ZSO/CNT-0/Ar. The crystallite hexagonal willemite phase was not achieved as the CNT concentration increased but semi-crystallite willemite phase was observed, and the crystallite size and the lattice strain were calculated. The calculated lattice strain (ε_{exp}, ε_{WH} and ε_0) increased as the crystallite size (τ_{exp}, τ_{WH} and τ_0) of willemite phase was decreased (table 3). Semi-crystallite willemite phase and amorphous state in ZSO/CNT-x/atm with increasing CNT showed great in lattice strain as the silicate ion was partly reacted with the exposed cobalt after the graphite layers was invaded by oxygen radical at high temperature. Glassy cobalt-silicate compound reduced the crystalline phase of zinc-silicate towards willemite phase formation.

Reducing lattice strain (lattice distortion and imperfections in crystal matrix) with enhancing the crystallite size was reported in [29, 30], showing the relationship of crystallite size and lattice strain. CNT with high thermal conductivity (600–750 W mK^{-1}) and high melting point (>3000 °C) enhance the thermal energy transport from the external heat source (heating coil of the furnace) to the host matrix without changing the carbon structure leads to enhance the crystallite size [2, 31]. Near homogenized distribution of 3 wt% CNT in ZSO/CNT-3/Ar composite showed the least phase left-shifting and resulted the reduced lattice strain with enlarging crystallite size without changing the domain phase of crystal.

3.2. Microscopic observation and element distribution

Figure 8 shows the morphology of the ZSO/CNT/Ar which is observed by FESEM. Figure 8(e) shows microscopy image of CNT with worm-liked fibrous structure (averaged diameter 23.08 ± 5.45 nm), similar with CNT [32, 33] and carbon bulks structure exist in the sample, which is in agreement to XRD results. CNT are crystalline carbon plane with hexagonal structure and rolled into tubular shape while amorphous carbon shows random orientation of carbon particle. The nano sized of CNT and the dominating amorphous carbon are the reasons behind obtaining a broadening carbon peak from the XRD spectrum.

From figures 8(a)–(d), the surface morphology of ZSO/CNT-x/Ar were observed. CNT was well dispersed into the glass powder as the non-uniform morphology and size of the glass particle due to the manual crushing and grinding process (particle size distribution refers to table 4). The size of CNT was relatively small (nano-sized) to the glass particle (micron-sized) as the CNT capable to fill in the gap between the glass particle. CNT filled in the gap between the glass particle in form of bundle as shown in inset image of figures 8(a)–(d). This showed the agglomeration of the CNT due to the small size of the cobalt catalyst and the CNT. Cobalt particles and nanotubes needed energy to achieve thermodynamically stable which cannot be achieved individually due to small size. During agglomeration in dry powder state, individual nanotubes and particles contribute energy and shared with neighbours to overcome energy insufficient [34, 35]. Figure 9 shows the morphology of ZSO/CNT-x/atm. There is agglomeration of cobalt particles (smaller particles, 66.754 ± 24.807 nm) without worm like structure attached on the semi-crystallite glass grain (bigger particles, 123.37 ± 76.89 nm). Semi-crystallite and glassy structure below crystallite temperature obtained insufficient energy in nucleation but sufficient energy in melting and fusing, comes with greater particle size compare to ZSO/CNT-0/atm (2.95 ± 0.10 μm). The detailed particle size distribution of ZSO/CNT-x/Ar and ZSO/CNT-x/atm were displayed in table 4.

Elemental analysis of the composite was done via EDS detector onto five sample: ZSO/CNT-0/Ar, ZSO/CNT-3/Ar, ZSO/CNT-0/atm, ZSO/CNT-3/atm and CNT (figures 10(a)–(e)). Atomic ratio of carbon to cobalt is about 6:1, means one mol of cobalt atom capable in producing six mol of carbon nanomaterials. ZSO/CNT-0/Ar without any addition of CNT results 16.15 at% of carbon content referring to table 5. This is believed due to the manufacturing of glass bottle is exposed to atmospheric carbon content as the carbon atom diffuse into the glass and the remaining PVA binding agent. Impurities like 3.71% aluminium is believed to be the mechanical properties enhancer during the manufacturing of glass bottle [26]. The ratio 1:3 of Si: Zn is due to the 60% SiO_2 in SLS glass reacts with mass ratio 1:1 of ZnO. Table 5 showed the carbon content dominating the other elements, having a composition of 61.05% with 3 wt% CNT added. The density of CNT is low [36], while the volume of CNT added is large with 3 wt% per mass of ZnO/SLS powder. The impurified CNT contains not only CNT, but amorphous carbon and different carbon nanomaterials.

Table 3. W-H equation calculated crystallite size (τ_{WH} and τ_0 in nm) and lattice strain (ε_{WH} ($\times 10^{-3}$) and ε_0 ($\times 10^{-3}$)) of ZSO/CNT-x/atm and Scherrer equation calculated crystallite size (τ_{exp} in nm) and lattice strain (ε_{exp} ($\times 10^{-3}$)) as comparison. Change of crystallite size and lattice strain (%) for CNT-added sample was calculated respected to ZSO/CNT-0/atm.

	Williamson-Hall equation calculated								Scherrer equation calculated			
atm sintered sample	τ_{WH}	ε_{WH}	τ_{WH}(%)	ε_{WH}(%)	τ_0	ε_0	τ_0(%)	ε_0(%)	τ_{exp}	ε_{exp}	τ_{exp}(%)	ε_{exp}(%)
ZSO/CNT-0	109.27	0.63	—	—	60.60	1.35	—	—	63.61	1.52	—	—
ZSO/CNT-1	78.85	0.48	−38.58	−24.27	45.35	2.07	−25.16	+53.33	60.42	2.14	−5.02	+40.94
ZSO/CNT-2	37.71	−0.01	−90.76	−100.83	37.81	2.57	−37.60	+90.37	41.95	3.39	−34.04	+123.17
ZSO/CNT-3	15.66	−0.87	−118.72	−237.52	18.43	4.07	−69.59	+201.48	18.52	6.18	−70.88	+306.95

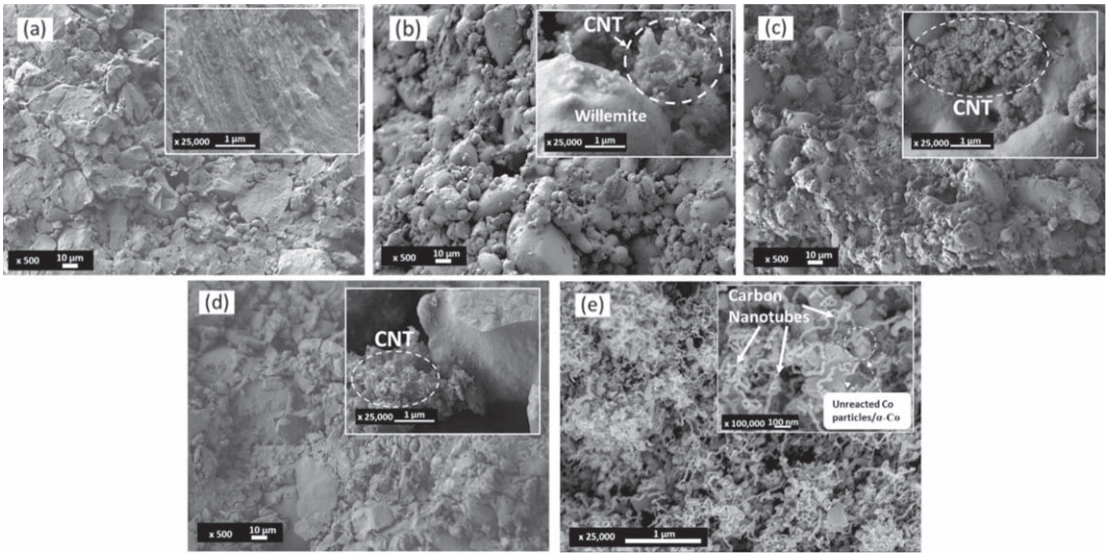

Figure 8. FESEM micrograph of (a)–(d) ZSO/CNT-x/Ar with x = 0, 1, 2, and 3 wt% and (e) synthesised CNT. The inset of (a)–(d) show high magnification of ×100 000 while the inset of (e) show magnification of ×25 000.

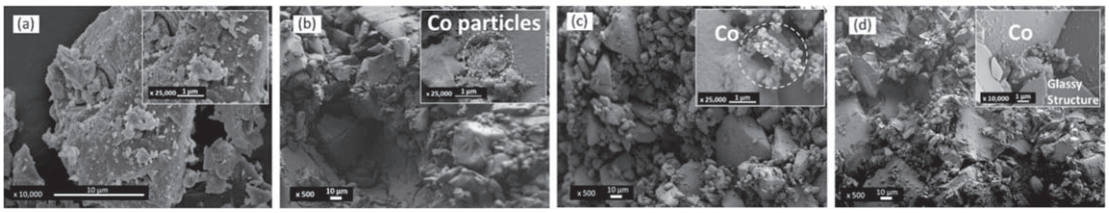

Figure 9. FESEM micrograph of atmospheric sintered ZSO/CNT-x: (a)–(d) 0, 1, 2 and 3 wt% CNT addition. The inset of (a)–(c) show high magnification of ×100 000 while the inset of (d) show magnification of ×10 000. Glassy ZSO/CNT-3/atm composite with poor electron conductive characteristics resulted blurry micrograph above ×10 000 magnification.

Table 4. CNT diameter, Co and ZSO particle sizes distribution in ZSO/CNT-x composite.

Sample	Particle size (μm)
ZSO/CNT-0/Ar	16.83 ± 12.60
ZSO/CNT-1/Ar	17.31 ± 8.75
ZSO/CNT-2/Ar	16.54 ± 6.44
ZSO/CNT-3/Ar	19.64 ± 8.74
ZSO/CNT-0/atm	2.95 ± 0.10
ZSO/CNT-1/atm	19.21 ± 7.46
ZSO/CNT-2/atm	123.37 ± 76.90
ZSO/CNT-3/atm	125.46 ± 60.49
Co particle (nm)	66.75 ± 24.81
CNT diameter (nm)	23.08 ± 5.45

4. Conclusions

In this study, ZSO/CNT composite was successfully synthesized via dry powder processing technique. Introduction of 3 wt% CNT into ZSO helped in reducing lattice strain of crystallite willemite phase for 22.85% as compared to ZSO without CNT addition. The willemite phase remained unchanged while sintered with higher CNT concentration in Argon gas environment. Atmospheric sintered sample with increasing CNT addition resulted in amorphous structure as the cobalt catalyst reacted with the silicate domain, resulted glassy structure with higher crystallite temperature. We concluded dry powder processing and inert gas sintering

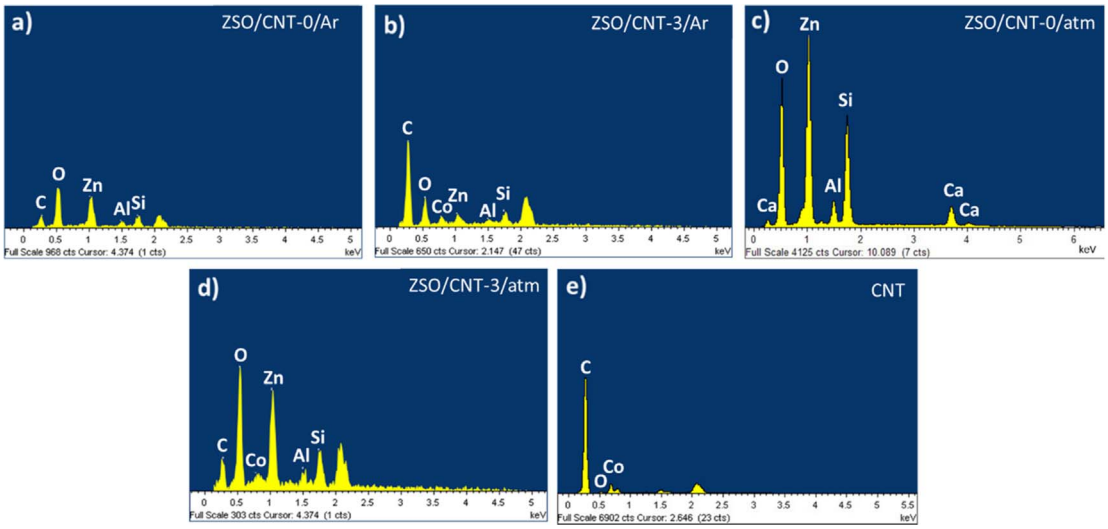

Figure 10. EDX spectrum of argon sintered ZSO/CNT with (a) without CNT addition and (b) with 3 wt% CNT addition, atmospheric sintered ZSO/CNT with (c) without CNT addition and (d) with 3 wt% CNT addition, and synthesised CNT.

Table 5. Element Analysis of sintered pellet and CNT.

	Element composition (wt%)						
Sample	C	O	Al	Si	Ca	Co	Zn
ZSO/CNT-0/Ar	18.22	39.30	4.95	8.84	—	—	28.69
ZSO/CNT-3/Ar	66.06	13.75	2.29	5.07	—	11.77	1.06
ZSO/CNT-0/atm	—	37.64	3.10	14.90	4.34	—	40.02
ZSO/CNT-3/atm	17.28	33.98	3.26	9.67	—	14.57	21.23
CNT	86.36	2.11	—	—	—	3.39	—

process can be efficient in introducing CNT into glassy zinc silicate and phase-changed into crystallite willemite with limiting lattice strain and preserving the domain phase.

Acknowledgments

This research was supported by Malaysia Ministry of Education (MoE) through Fundamental Research Grant Scheme (FRGS/1/2018/STG07/UPM/02/3) No. 5540132 and Universiti Putra Malaysia (UPM) under Inisiatif Putra Muda (GP-IPM/2017/9543800).

ORCID iDs

Kar Fei Chan https://orcid.org/0000-0003-3333-814X
Mohd Hafiz Mohd Zaid https://orcid.org/0000-0001-6734-800X
Shahira Liza https://orcid.org/0000-0002-5282-1893
Yazid Yaakob https://orcid.org/0000-0001-6691-433X

References

[1] Holubowitch N E, Landon J, Lippert C A, Craddock J D, Weisenberger M C and Liu K 2016 Spray-coated multiwalled carbon nanotube composite electrodes for thermal energy scavenging electrochemical cells *ACS Appl. Mater. Interfaces* **8** 22159–67
[2] Jiang L and Gao L 2008 Densified multiwalled carbon nanotubes-titanium nitride composites with enhanced thermal properties *Ceram. Int.* **34** 231–5
[3] Boulerouah A, Longuemart S, Hus P and Sahraoui A H 2013 Thermal transport investigation in a CNTs/solid matrix composite *J. Phys. D: Appl. Phys.* **46** 055302
[4] Giovanardi R, Montorsi M, Ori G, Cho J, Subhani T, Boccaccini A R and Siligardi C 2010 Microstructural characterisation and electrical properties of multiwalled carbon nanotubes/glass-ceramic nanocomposites *J. Mater. Chem.* **20** 308–13

[5] Peng B, Takai C, Razavi-Khosroshahi H, Salmawy M S E and Fuji M 2018 Effect of CNTs on morphology and electromagnetic properties of non-firing CNTs/silica composite ceramics *Adv. Powder Technol.* **29** 1865–70
[6] Yoshio S, Tatami J, Wakihara T, Yamakawa T, Nakano H, Komeya K and Meguro T 2011 Effect of CNT quantity and sintering temperature on electrical and mechanical properties of CNT-dispersed Si_3N_4 ceramics *J. Ceram. Soc. Japan* **119** 70–5
[7] Indora V, Yadav S and Mohan D 2020 *Optical and Structural Analysis of Sol-gel Derived TiO_2/MWCNT Nanocomposites* **2220** 020110
[8] Wongaree M, Chiarakorn S and Chuangchote S 2015 Photocatalytic improvement under visible light in TiO_2 nanoparticles by carbon nanotube incorporation *J. Nanomater.* **2015** 1–10
[9] Cho J, Boccaccini A R and Shaffer M S P 2009 Ceramic matrix composites containing carbon nanotubes *J. Mater. Sci.* **44** 1934–51
[10] Lamnini S, Károly Z, Bódis E, Balázsi K and Balázsi C 2019 Influence of structure on the hardness and the toughening mechanism of the sintered 8YSZ/MWCNTs composites *Ceram. Int.* **45** 5058–65
[11] Zhang X, Li S, Pan B, Pan D, Liu L, Hou X, Chu M, Kondoh K and Zhao M 2019 Regulation of interface between carbon nanotubes-aluminum and its strengthening effect in CNTs reinforced aluminum matrix nanocomposites *Carbon N. Y.* **155** 686–96
[12] Yamamoto G, Shirasu K, Nozaka Y, Wang W and Hashida T 2014 Microstructure-property relationships in pressureless-sintered carbon nanotube/alumina composites *Mater. Sci. Eng.* A **617** 179–86
[13] Xu R, Tan Z, Xiong D, Fan G, Guo Q, Zhang J, Su Y, Li Z and Zhang D 2017 Balanced strength and ductility in CNT/Al composites achieved by flake powder metallurgy via shift-speed ball milling *Compos. Part A Appl. Sci. Manuf.* **96** 57–66
[14] Liu Z Y, Zhao K, Xiao B L, Wang W G and Ma Z Y 2016 Fabrication of CNT/Al composites with low damage to CNTs by a novel solution-assisted wet mixing combined with powder metallurgy processing *Mater. Des.* **97** 424–30
[15] Mazaheri M, Mari D, Schaller R, Bonnefont G and Fantozzi G 2011 Processing of yttria stabilized zirconia reinforced with multi-walled carbon nanotubes with attractive mechanical properties *J. Eur. Ceram. Soc.* **31** 2691–8
[16] Bi S, Hou G, Su X, Zhang Y and Guo F 2011 Mechanical properties and oxidation resistance of α-alumina/multi-walled carbon nanotube composite ceramics *Mater. Sci. Eng.* A **528** 1596–601
[17] Zaid M H M, Matori K A, Quah H J, Lim W F, Sidek H A A, Halimah M K, Yunus W M M and Wahab Z A 2015 Investigation on structural and optical properties of SLS–ZnO glasses prepared using a conventional melt quenching technique *J. Mater. Sci., Mater. Electron.* **26** 3722–9
[18] Duddu S P, Fung F K Y and Grant D J W 1996 Effects of crystallization in the presence of the opposite enantiomer on the crystal properties of (SS)-(+)-pseudoephedrinium salicylate *Int. J. Pharm.* **127** 53–63
[19] Tatsumisago M, Okuda K, Itakura N and Minami T 1999 Crystallization of α-AgI from AgI–Ag_2O–M_xO_y (M_xO_y = B_2O_3, GeO_2, WO_3) melts and glasses *Solid State Ionics* **121** 193–200
[20] Wu Y, Chen Z, Nan P, Xiong F, Lin S, Zhang X, Chen Y, Chen L, Ge B and Pei Y 2019 Lattice strain advances thermoelectrics *Joule* **3** 1276–88
[21] Nisar A, Ariharan S, Venkateswaran T, Sreenivas N and Balani K 2017 Effect of carbon nanotube on processing, microstructural, mechanical and ablation behavior of ZrB2-20SiC based ultra-high temperature ceramic composites *Carbon N. Y* **111** 269–82
[22] Smith A M, Mohs A M and Nie S 2009 Tuning the optical and electronic properties of colloidal nanocrystals by lattice strain *Nat. Nanotechnol.* **4** 56–63
[23] Williamson G K and Hall W H 1953 X-ray line broadening from filed aluminium and wolfram *Acta Metall.* **1** 22–31
[24] Scherrer P 1918 Bestimmung der Größe und der inneren Struktur von Kolloidteilchen mittels Röntgenstrahlen *Nachrichten von der Gesellschaft der Wissenschaften zu Göttingen, Math. Klasse* **2** 98–100
[25] Kazemnejad I, Feizbakhsh A, Niazi A and Tavasoli A 2019 Highly dispersed cobalt Fischer–Tropsch synthesis catalysts supported on γ-Al_2O_3, CNTs, and graphene nanosheet using chemical vapor deposition *Int. J. Ind. Chem.* **10** 321–33
[26] Shiflet G J, Leng Y and Hawk J W 2000 Metallic glasses *Ullmann's Encyclopedia of Industrial Chemistry* vol 41 (Weinheim, Germany: Wiley-VCH Verlag GmbH & Co. KGaA) pp 369–87
[27] Potoczna-Petru D and Krajczyk L 2003 Spreading of cobalt phase and silicate formation in Co/SiO_2 model catalyst *Catal. Letters* **87** 51–6
[28] Wahab S A A, Matori K A, Aziz S H A, Zaid M H M, Kechik M M A, Azman A Z K, Khaidir R E M, Khiri M Z A and Effendy N 2019 Synthesis of cobalt oxide Co_3O_4 doped zinc silicate based glass-ceramic derived for LED applications *Optik (Stuttg)* **179** 919–26
[29] Kurian M and Kunjachan C 2014 Investigation of size dependency on lattice strain of nanoceria particles synthesised by wet chemical methods *Int. Nano Lett.* **4** 73–80
[30] Muhammed Shafi P and Chandra Bose A 2015 Impact of crystalline defects and size on x-ray line broadening: a phenomenological approach for tetragonal SnO_2 nanocrystals *AIP Adv.* **5** 057137
[31] Xie H, Cai A and Wang X 2007 Thermal diffusivity and conductivity of multiwalled carbon nanotube arrays *Phys. Lett. Sect. A Gen. At. Solid State Phys.* **369** 120–3
[32] Abdulrazzak F, Abbas A and Hussein F 2017 Synthesis of few-wall carbon nanotubes using methanol/ propanol mixture by chemical vapour deposition *Front. Nanosci. Nanotechnol.* **3** 1–7
[33] Ibrahim R, Hussein M Z, Yusof N A and Bakar F A 2019 Carbon nanotube-quicklime nanocomposites prepared using a nickel catalyst supported on calcium oxide derived from carbonate stones *Nanomaterials* **9** 1239
[34] Li Q, Church J S, Kafi A, Naebe M and Fox B L 2014 An improved understanding of the dispersion of multi-walled carbon nanotubes in non-aqueous solvents *J. Nanoparticle Res.* **16** 2513
[35] Groza J R 1999 Nanosintering *Nanostructured Mater.* **12** 987–92
[36] Bierdel M, Buchholz S, Michele V, Mleczko L, Rudolf R, Voetz M and Wolf A 2007 Industrial production of multiwalled carbon nanotubes *Phys. Status Solidi Basic Res.* **244** 3939–43